The 2015 World Congress on
Advances in Civil, Environmental, and Materials Research (ACEM15)
Incheon, Korea, August 25-29, 2015

Finite element and neural network model of electrical capacitance sensor to simulate the pipelines suffer from internal corrosion

*Wael A. Al-Tabey[1)]

Department of Mechanical Engineering, Alexandria University, Alexandria (21544), Egypt
wael.altabey@gmail.com

ABSTRACT

As the study of internal corrosion of pipeline need a large number of experiments as well as long time, so there is a need for new computational technique to expand the spectrum of the results and to save time. The present work represents two techniques to detect the corrosion rates inside steel pipelines and study and predict the effect of pipeline environment temperature (θ) on the corrosion rates increases. The first technique is electrical capacitance tomography (ECT) sensor, ECT sensor is consists of number of electrodes mounted on the outer surface of pipeline, radius-electrode ratio is defined as the ratio of inner and outer radius of pipeline. The rules of 24-electrode sensor parameters such as capacitance, capacitance change, and change rate of capacitance are discussed by ANSYS and MATLAB. The second technique is a feed-forward neural network (FFNN) structure are applied, trained and tested to predict the corrosion rates under different temperature using MATLAB neural network toolbox. The groups of data considered are the corrosion rates and the ECT excitation voltage (φ) with the different pipeline environment temperature (θ). Evaluation and analysis of the results leads to better understanding of the corrosion mechanism under different environmental temperature.

1. INTRODUCTION

Pipelines play an extremely important role throughout the world as means of transporting gases and liquids over long distances from their sources to the ultimate consumers. Pipelines suffer from corrosion, cracking and other problems. Internal corrosion has been recognized for many years as one of the main deterioration mechanisms that may reduce the structural properties of transmission pipelines.

ECT sensor was first introduced in the 1980s by a group of researchers from the US Department of Energy Morgantown Energy Technology Center (METC), to measure fluidized bed system (Fasching et al, 1988, Fasching et al, 1991).

ECT sensor is one of the most mature and promising methods, which measures the capacitance change of multi-electrode sensor due to the change of dielectric permittivity being imaged, and then reconstructs the cross-section images using the measured raw data with a suitable algorithm. It has the characteristics such as low cost,

---

[1)] Assistant Professor

fast response, non-intrusive method, broad application, safety (Yang et al., 1995a, 1995b, Li Haiqing et al., 2000). ECT system includes sensor, capacitance measuring circuit and imaging computer is shown in Fig.1. And ECT sensor consists of insulating pipeline, measurement electrode, radial screen and earthed screen (Yang et al., 1999). The measurement electrode is mounted symmetrically around the circumference of pipeline. Radial screen is fitted between the electrodes to cut the electro line external to the sensor pipeline and reduce the inter-electrode capacitance. The earthed screen surrounds the measurement electrodes to shield external electromagnetic noise. ECT sensor converts the permittivity of inner media flow to inter-electrode capacitance, which is the ECT forward problem. Capacitance measuring circuit takes the capacitance data and transfers to imaging computer. Imaging computer reconstructs the distribution image with a suitable algorithm, which is called ECT inverse problem.

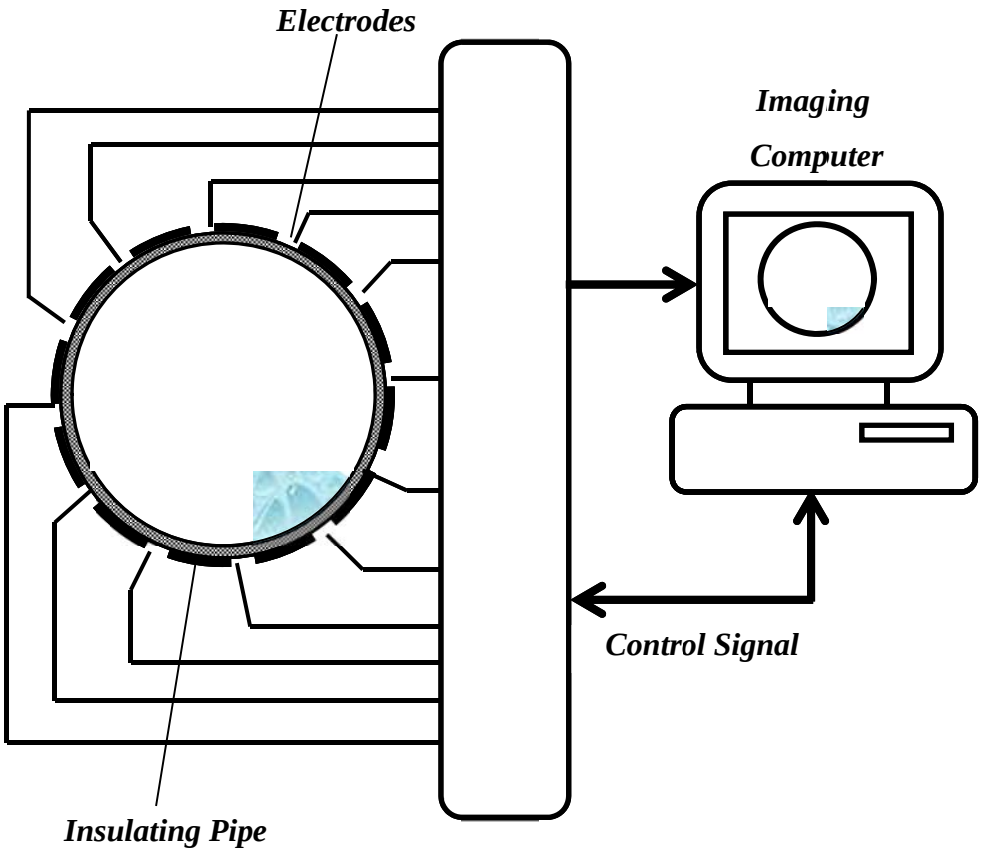

Fig. 1 Sketch of ECT system

In most application, ECT electrode is mounted outside the ECT pipeline which is called external electrode ECT sensor (Yang et al., 1997), so pipeline thickness is a very important parameter in ECT sensor design. There are three factors which have great effect on ECT sensor measurements, e.g. pipeline material, inner dielectric permittivity and the ratio of pipeline thickness and diameter (Jaworski et al., 2000).

Finite element (FE) method has been widely used to numerically solve mathematical problems in many engineering fields (Xie et al., 1992). Hence characteristic 24-

electrode ECT sensor with different pipeline thickness is studied in the method of numerical simulation to simulate the pipelines suffer from internal corrosion problem at normal temperature equal to 25℃ in which ANSYS is combined with MATLAB. The main goal of the artificial neural network (ANN) design is predicting non- FE data not included in FE evaluation to expand the spectrum of the results and to save time effort. The effect of pipeline environment temperature (θ) on the corrosion rates increases, (i.e. the capacitance change measurements), is studied under three deferent temperatures by using the feed-forward neural network (FFNN). In the first the FFNN is trained and tested to predict some of FE data, then we will use the suggested FFNN to predict some non- FE data of the corrosion rates under three different pipeline temperatures. On the other hand, more accurate prediction method is obtained by using a useful expert system which is designed to aid the designer to decide whether his suggested data for the corrosion rates is suitable or not.

2. ELECTRICAL CAPACITANCE TOMOGRAPHY ECT SENSOR MODEL

2.1 The ECT sensor geometrical model

For a sensor with N electrodes are installed on the outer wall symmetrically along the circumference of pipe, there are $N(N-1)/2$ electrode pairs, hence $N(N-1)/2$ independent capacitance measurements. Fig.2 is the partial from cross section of 24-electrode ECT sensor, in which R_1 is inner pipeline radius; R_2 is outer pipeline radius; X is the pipe wall thickness; R_3 is earthed screen radius; and radial screen is connected to outer pipeline.

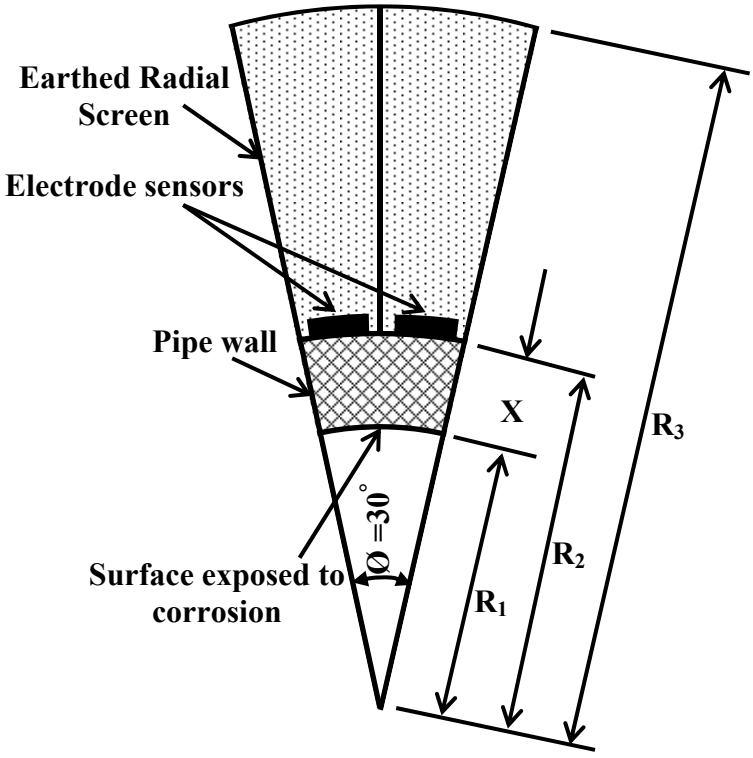

Fig. 2 The partial cross section sketch of ECT sensor

For the purpose of making the describe of pipeline corrosion (wall thickness) easier, the concept of radius-electrode ratio ρ ($\rho = R_1/R_2$) is put backward, which is the ratio of pipeline inner radius to electrode radius (i.e. pipeline outer radius). In ideal condition (No corrosion), pipeline wall thickness is X = (R_2-R_1), so ρ is equal to constant value of R_1/R_2. The larger radius-electrode ratio is, the more serious the effect of pipeline corrosion becomes.

2.2 The ECT sensor mathematical model

The system model for *ECT* system is based on the electrostatic field theory, which can be used to find the potential distribution $\varphi(\mathrm{x},\mathrm{y})$ inside the ECT sensor. By solving the Poisson's equation:

$$\nabla.\,\varepsilon(x,y)\nabla.\,\varphi(x,y) = 0 \tag{1}$$

For the boundary condition imposed on the ECT sensor head by the measurement system, the potential distribution $\varphi(\mathrm{x},\mathrm{y})$ can be found. The electric field vector $\mathrm{E}(\mathrm{x},\mathrm{y})$ and the potential function $\varphi(\mathrm{x},\mathrm{y})$ are related as follows:

$$\mathrm{E}(\mathrm{x},\mathrm{y}) = -\nabla\varphi(\mathrm{x},\mathrm{y}) \tag{2}$$

The change on the electrodes, and hence the inter electrode capacitances can be found using the definition of the capacitance and Gauss's law based on the following surface integral:

$$\mathrm{Q_{ij}} = \oint_{\mathrm{S_j}} (\varepsilon(\mathrm{x},\mathrm{y})\nabla\varphi(\mathrm{x},\mathrm{y}).\,\hat{\mathrm{n}})\,\mathrm{ds} \tag{3}$$

Where: $\varphi(\mathrm{x},\mathrm{y})$ is potential distribution, $\varepsilon(\mathrm{x},\mathrm{y})$ is permittivity distribution, $\mathrm{E}(\mathrm{x},\mathrm{y})$ is electric field vector, $\nabla.$ is divergence operator, ∇ is gradient operator, $\mathrm{S_j}$ is a surface enclosing electrode j, $\mathrm{d}s$ is an infinitesimal area on electrode j and $\hat{\mathrm{n}}$ is the unit vector normal to $\mathrm{S_j}$. Using these charge measurements $\mathrm{Q_{ij}}$, the inter electrode capacitance $\mathrm{C_{ij}}$ can be compute using the definition of Eq.(4):

$$\mathrm{C_{ij}} = \frac{\mathrm{Q_{ij}}}{\Delta\mathrm{V_{ij}}} \tag{4}$$

Where $\mathrm{Q_{ij}}$ is the charge induced on electrode (j) when electrode (i) is excited with a known potential, $\Delta\mathrm{V_{ij}}$ is the potential difference between electrodes (i) and (j) $\left(\Delta\mathrm{V_{ij}} = \mathrm{V_i} - \mathrm{V_j}\right)$.

2.3 The ECT sensor composition and working principle

When one electrode is excited, the other electrodes are kept at ground potential as shown in the Fig.3 and act as detector electrodes. When electrode No. 1 is excited with a potential, the change $\mathrm{Q_{1,j}}$ is induced on the electrodes, $\mathrm{j} = 2,\cdots\cdots,\mathrm{N}$ can be

measured. Next, electrode No. 2 is excited whereas, rest the electrodes are kept at ground potential, and the induced charges $Q_{23}, Q_{24}, \cdots, Q_{2N}$ are measured. The measurement protocol continues unit electrode N-1 is excited.

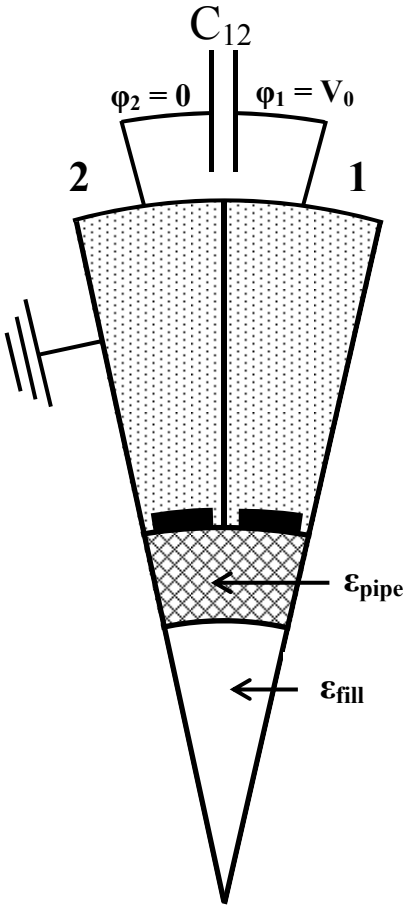

Fig. 3 Schematic representation of the measurement principle of an ECT sensor

4. FINITE ELEMENT METHOD (FEM) OF ECT SENSOR

Solving Eq.(1), the sensor potential distribution $\varphi(x, y)$ can be obtained. For the structure irregularity of sensor electrode pair and the in-homogeneity of dielectric distribution, Eq.(1) doesn't exist analytical solution, but it can be worked out through FEM. When using FEM to solve problem, the continuous field should be converted to a discrete form, namely, the solution domain should be divided into finite elements. For the convenience of numerical simulation, the FEM software ANSYS is used to build the geometry model of sensor and divide the cross section domain into triangle elements, see Fig.4. The partition results such as node coordinates, boundary condition and relation between elements and nodes are extracted to calculate potential distribution in MATLAB.

4.1 Boundary conditions

The potential boundary conditions were applied to the sensor-plate (electrodes). For one electrode, the boundary condition of electric potential ($V=V_0$) with 15V (V_0) was applied and another electrode was kept at ground (V=0) potential to simulate a 15V (rms) potential gradient across the electrodes.

4.2 The Geometric Properties

For empty pipeline of steel, we will get the distribution of electric sensitive potential and effect of pipeline corrosion on the sensitive field. The simulation settings of steel and air relative permittivity ε is 7, and 1.0, respectively and set number 24 electrode excitation electrodes, excitation voltage V_0 = 15 volts, the sensor physical specification shown in Table (1). The remaining electrode and shield grounding, Simulation picture is as follows.

Table 1.Sensor physical specification

No. of electrodes	24	Thickness of electrodes	1mm
Guards between electrodes	1 mm	Permittivity pipe wall	ε_{pipe} = 7
Inner/outer pipe diameter	49.3/65.2 mm	Excitation voltage	φ = 15 Volts
Earth Screen diameter	120mm		

4.3 The Field Partition

According to finite element analysis, we will carry out imaging of regional triangulation, it is necessary to divided pixel pipelines into triangular finite element. Imaging region is divided into 997 Elements; the map is as follows in Fig.4.

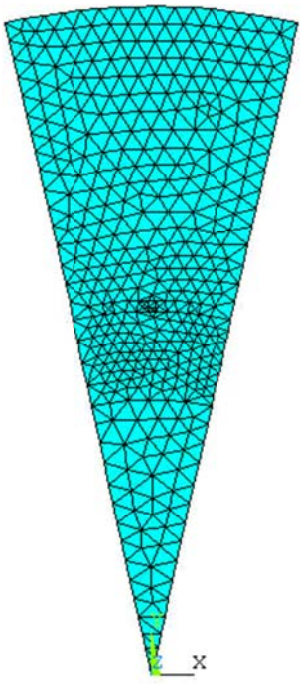

Fig.4 Element map of finite element mesh

The Simulations, and the node potential distribution of pipeline suffer from internal corrosion (pipe wall thickness decrease) at $\theta = 25℃$, when a constant current is injected between electrode 1 and 2 are illustrated in Fig.5. Red color represents high electric potential. Blue represent ground potential.

5. SIMULATION ANALYSIS OF PIPELINE CORROSION

The pipeline internal corrosion can occur when the pipe wall is exposed to water and contaminants in the filling fluid, such as chlorides. The nature and extent of the corrosion damage that may occur are functions of the concentration and particular combinations of these various corrosive constituents within the pipe, as well as of the operating conditions of the pipeline.

The pipeline internal corrosion is means decrease of the pipeline thickness at repeated time interval (i.e. the radius-electrode ratio ρ increases). This work is targeted for sensing the internal corrosion as it occurs to avoid the corrosion and cracking problems. So in this section we will be discussed the effect of pipeline internal corrosion on ECT sensor capacitance C_{ij} by decreasing of pipeline thickness X, or increasing of radius-electrode ratio ρ, and study the change in the electrode sensors capacitance.

The parameters of simulated ECT sensor, which used in pipeline, include inner radius R_1, outer radius R_2, earthed screen radius R_3, solid permittivity ε_{pipe} and filling layer permittivity ε_{fill}. The outer radius is constant. The pipeline thickness $X = (R_2-R_1)$ is selected as X_1 = 7.95 mm, X_2 = 6.95 mm, X_3 = 5.95 mm, X_4 = 4.95 mm, X_5 = 3.95 mm, X_6= 2.95 mm and X_7 = 1.95 mm respectively, on the other hand the radius-electrode ratio $\rho = (1-(X/ R_2))$ equal to 0.76, 0.79, 0.82, 0.85, 0.88, 0.91, 0.94 respectively.

5.1 Effect of Pipeline Corrosion on Sensor Capacitance

The effect of the pipeline internal corrosion on Capacitance change in Pico Farad (10^{-12}Farad) is calculated, and investigated. Because of symmetry, 24-electrode sensor has 12 typical structures of inter-electrode pair; hence only 12 inter electrode pairs (C_{1-2}, C_{1-3}, C_{1-4}, C_{1-5}, C_{1-6}, C_{1-7}, C_{1-8}, C_{1-9}, C_{1-10}, C_{1-11}, C_{1-12} and C_{1-13}) are listed, as showing in Fig.6.

The tendency curve of capacitance change against X is shown in Fig.6. In adjacent electrode pair, capacitance change increases monotonously with the increase of X or decrease ρ, and turns to decrease with the increase of X. However, there exist maximum points in non-adjacent electrode pairs, and all the maximum values are at the same position where X= 6.95 mm, ρ = 0.79. So sensor with this ρ is more suitable to capacitance measurement.

Using the exponential formula (5) to fit the FE results of capacitance change have proved its suitability by giving acceptable values for the correlation factor (C.F) are very near to unity. The values of four constants (a_{ij}), (b_{ij}), (k_{ij}) and (h_{ij}) at $\theta = 25℃$ are displayed in Table (3).

$$C_{ij} = a_{ij}e^{b_{ij}X} + k_{ij}e^{h_{ij}X} \quad (5)$$

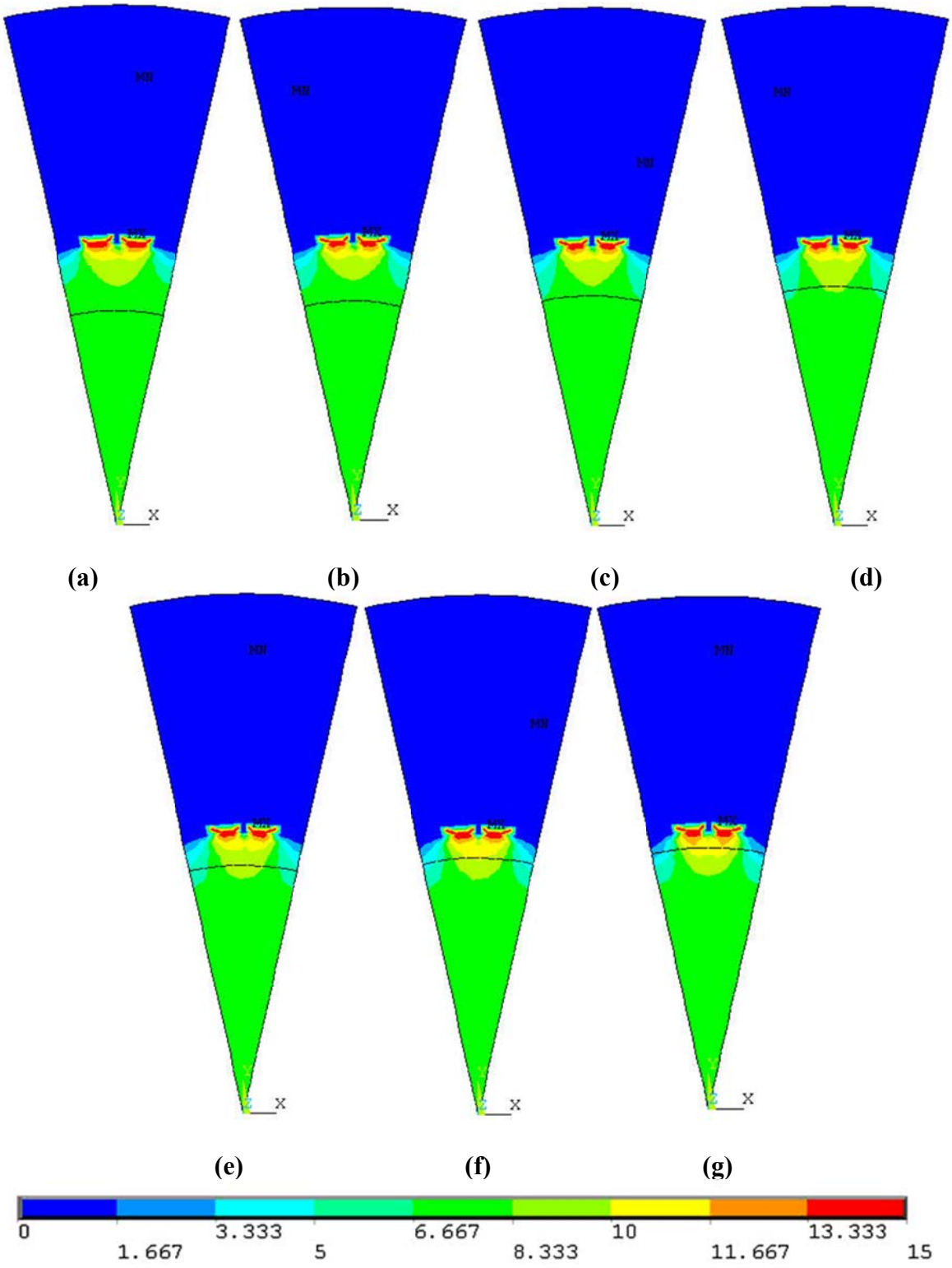

Fig.5 The node potential distribution of pipeline for decreasing of pipe wall thickness (i.e. corrosion behavior) at $\theta = 25℃$ (a) X_1 (b) X_2 (c) X_3 (d) X_4 (e) X_5 (f) X_6 (g) X_7

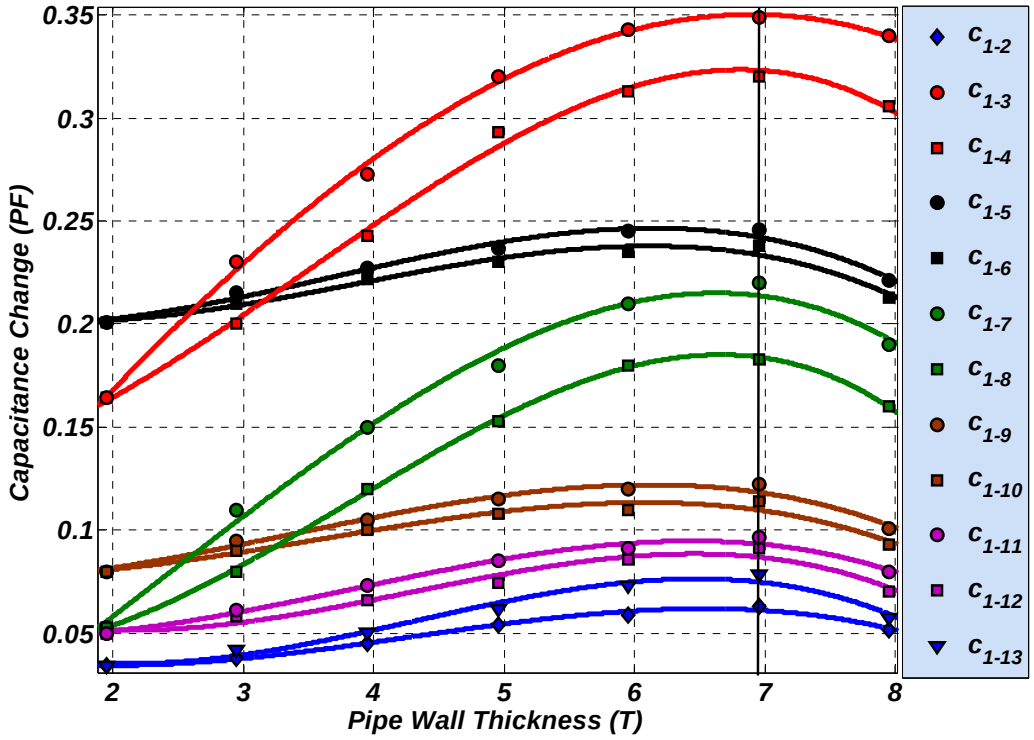

Fig.6 Effect of Pipeline Corrosion on Capacitance change at $\theta = 25℃$

6. ARTIFICIAL NEURAL NETWORK (ANN) MODEL FOR ECT TO STUDY THE EFFECT OF PIPELINE ENVIRONMENT TEMPERATURE (θ)

An ANN is designed to predict the corrosion rates (ECT capacitance change) of steel pipeline with radius-electrode ratio ρ, ECT excitation voltage φ under different pipeline environment temperature (θ), as the input and the corrosion rates as the output. A feed forward FFNN, is constructed, trained and tested.

6.1 A feed-forward Neural Network FFNN

A feed-forward NN is shown in Fig. 7. There is designed based on two layers, the first, input layer, has tan-sigmoid neurons while the second layer has pure linear ones. FFNN is trained by measuring values of ρ, φ, θ to predict corrosion rates. In the first FFNN structure is applied for training the data of ECT at normal temperature ($\theta = 25℃$). Fig.8 shows the training performance of suggested FFNN. Fig.9 represent the comparison between the FE data (ANSYS data) and the feed forward neural network FFNN predicted corrosion rates (ECT capacitance change) at ($\theta = 25℃$) for electrode pairs $C_{1\text{-}2}$ and $C_{1\text{-}13}$. The results of this NN show much satisfactory predication quality for this case study. Fig.10 shows the comparison between the FE data and the feed forward neural network FFNN expected data at($\theta = 25℃$) for electrode pairs $C_{1\text{-}7}$ and $C_{1\text{-}8}$. From this Figure, it noted that the expected data from the suggested FFNN are applicable with the FE data.

6.2 Neural System Validation and Reliability

It is very useful from the designer point of view to have an neural system aids to decide whether his suggested design for ECT structure is suitable or not by Compute the Mean Square error MSE from equation:

$$\mathrm{MSE} = \frac{\Sigma\left[(C_{ij})_{NN} - C_{ij}\right]^2}{n} \tag{7}$$

Where:

$(C_{ij})_{NN}$ is the predicted capacitance change,

C_{ij} is the capacitance change measured from FEM,

n is the number of FEM measured data values.

Table (2) gives the values of mean square error (MSE) (see Eq. (7)) between the expected and FE data for both FFNN predicted for electrode pairs $C_{1\text{-}2}$ and $C_{1\text{-}13}$ and FFNN expected data for electrode pairs $C_{1\text{-}7}$ and $C_{1\text{-}8}$, at($\theta = 25℃$) .

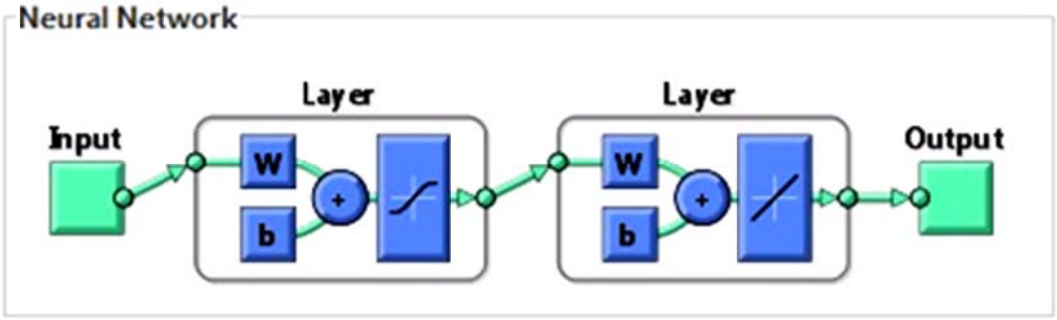

Fig.7 Schematic Illustration of FFNN design for present study with input data ρ, θ, φ

Table 2.Mean square error (MSE) values

$\theta = 25℃$		
Data	**Electrode pairs**	**MSE**
Predicted	$C_{1\text{-}2}$	7.6034 E-7
	$C_{1\text{-}13}$	4.3213 E-6
Expected	$C_{1\text{-}7}$	1.1835 E-5
	$C_{1\text{-}8}$	2.0552 E-5

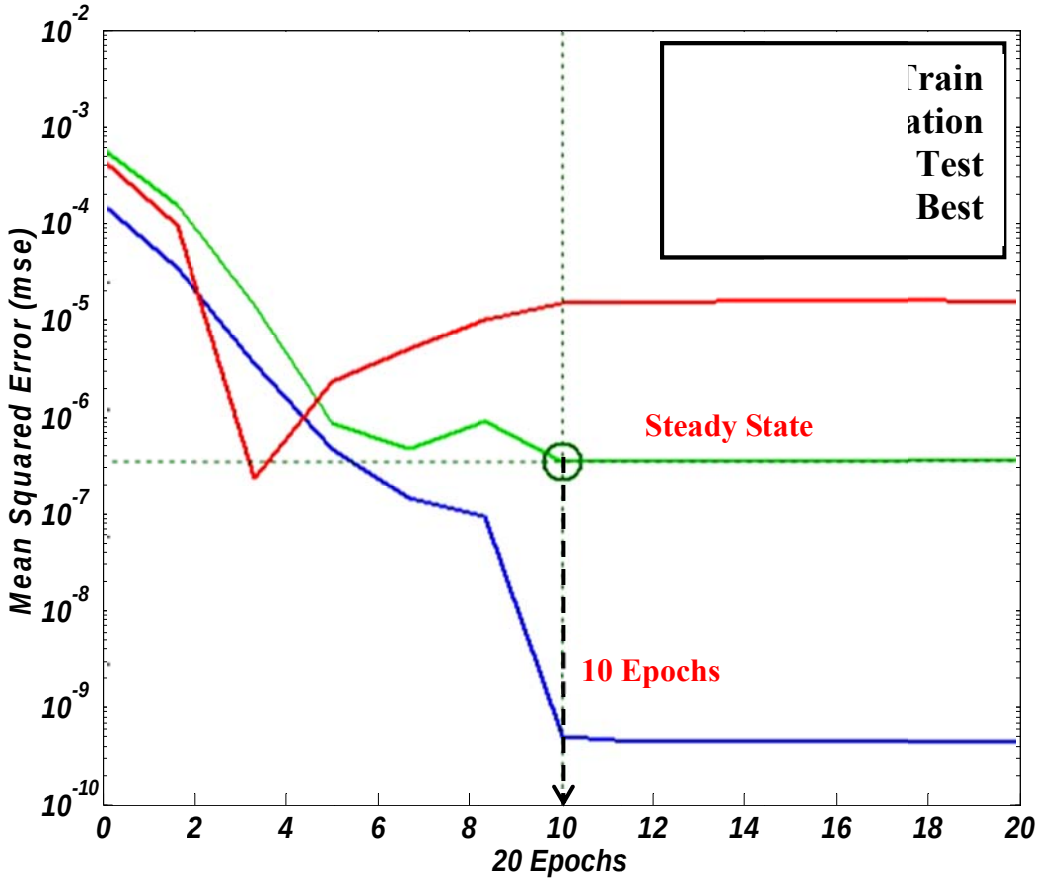

Fig.8 Training performance of suggested FFNN

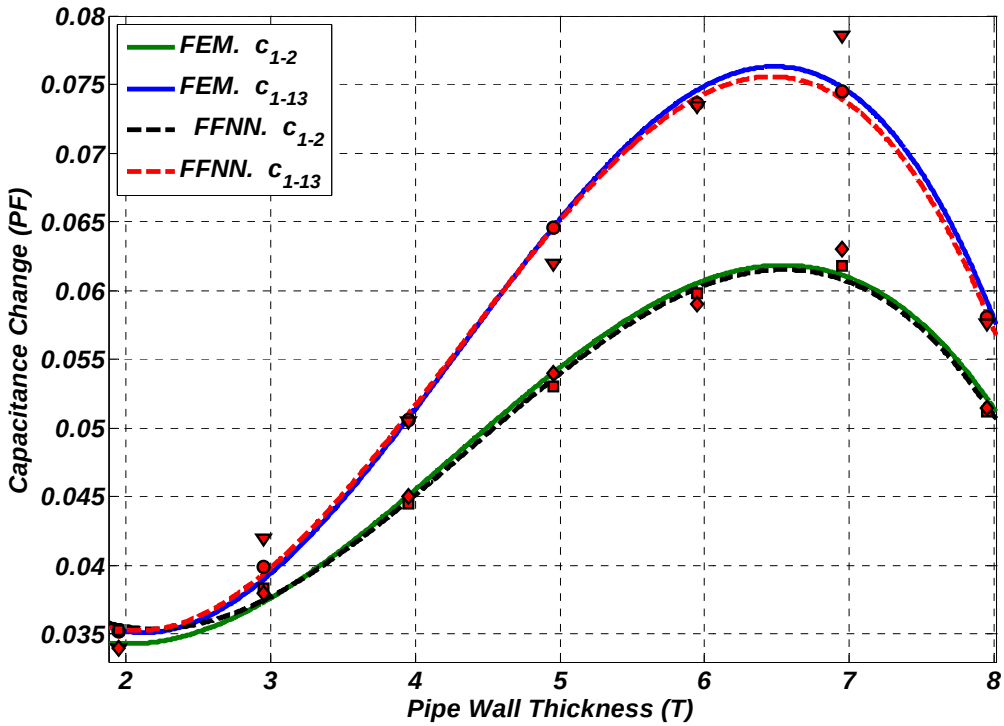

Fig.9 Comparison between the FE data and FFNN predicted data for $C_{1\text{-}2}$ and $C_{1\text{-}13}$ at $\theta = 25℃$

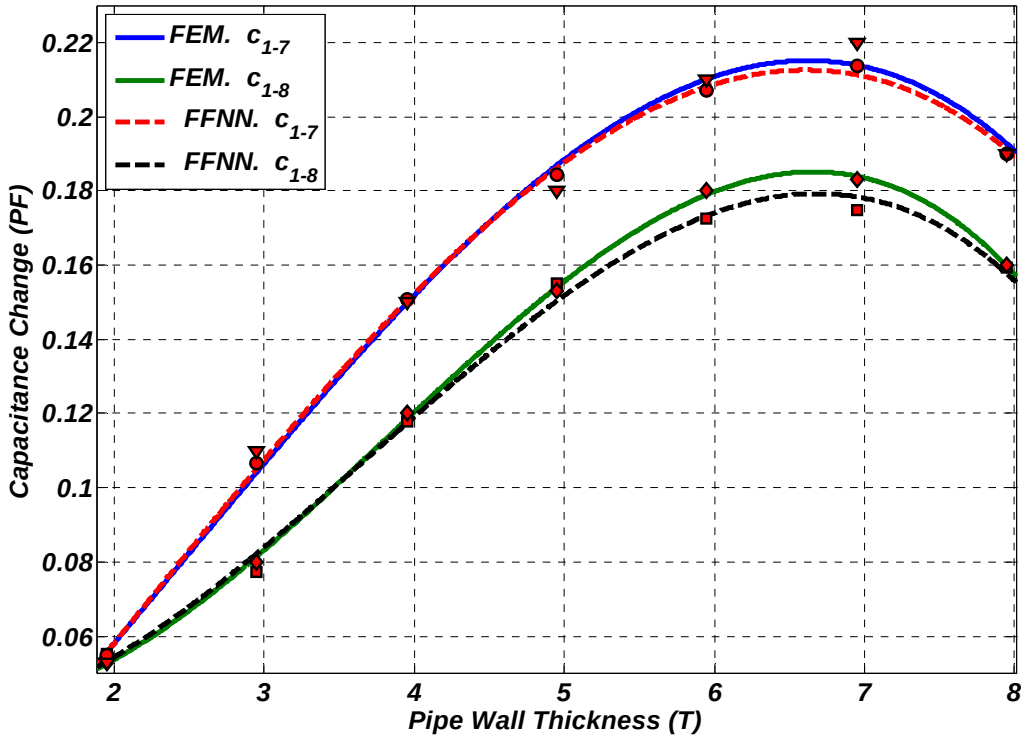

Fig.10 Comparison between the FE data and FFNN Expected data for C_{1-7} and C_{1-8} at $\theta = 25℃$

6.3 The Use of Present ANN in Predicting Non-FE Data

The main goal of the artificial neural network design is predicting non-FE data. In this section we will use the suggested FFNN to predict some non-FE data not included in FE evaluation. It is selected to use three different values of pipeline environment temperature (θ) of 40℃, 60℃ and 80℃ and random values of pipe wall thickness (X) for all electrode pairs C_{ij}. The previous three parameters are the input vectors for artificial neural network, while the output is the signal vector; the corrosion rates.

Fig.11 to Fig.13 represents the pipe wall thickness (X) against the capacitance change output from artificial neural network for all pipeline environment temperature (θ) of 40℃, 60℃ and 80℃ respectevely. Using the exponential formula $C_{ij} = a_{ij}e^{b_{ij}X} + k_{ij}e^{h_{ij}X}$ have proved its suitability by giving acceptable values for the correlation factors (C.F) are very near to unity.

Comparing the result predicted from artificial neural network and data obtained from FE method for the other values of pipeline environment temperature (θ), Table (3) it is conclude that the present artificial neural network is suitable and useful in predicting non-FE data.

6.4 the effect of pipeline environment temperature (θ)

Analyzing the values of four constants (a_{ij}), (b_{ij}), (k_{ij}) and (h_{ij}) taking into account the variation of pipeline environment temperature (θ), capacitance change (C_{ij}), and pipeline thickness (X) or radius-electrode ratio ρ, and considering Table (3) resulted in the following:

1) For all pipeline environment temperature (θ), at maximum points, the tendency curve of capacitance change against X for capacitance change (C_{1-3}) has the highest capacitance

change, the tendency curve for capacitance change (C_{1-2}) has the lowest capacitance change, while the other curves for the remaining capacitance change laid in between, with descending order from (C_{1-4}) to (C_{1-13}).

2) The values of the constants (a_{ij} & k_{ij}) were found to depend on the pipeline environment temperature (θ) for capacitance change (C_{ij}), as the pipeline environment temperature (θ) increases the absolute value of (a_{ij} & k_{ij}) will decreases, i.e. the capacitance change increased, means the corrosion rates increased.
3) The deviation in the values of the constants (b_{ij} & h_{ij}) at all pipeline environment temperature (θ) is negligible and it may be considered constant, the average value (Avg.) of constants (b_{ij} & h_{ij}) was calculated and considered to be used at any temperature (θ), as the corresponding standard deviation (S.D) was found to have acceptable values, as shown in Table (3).

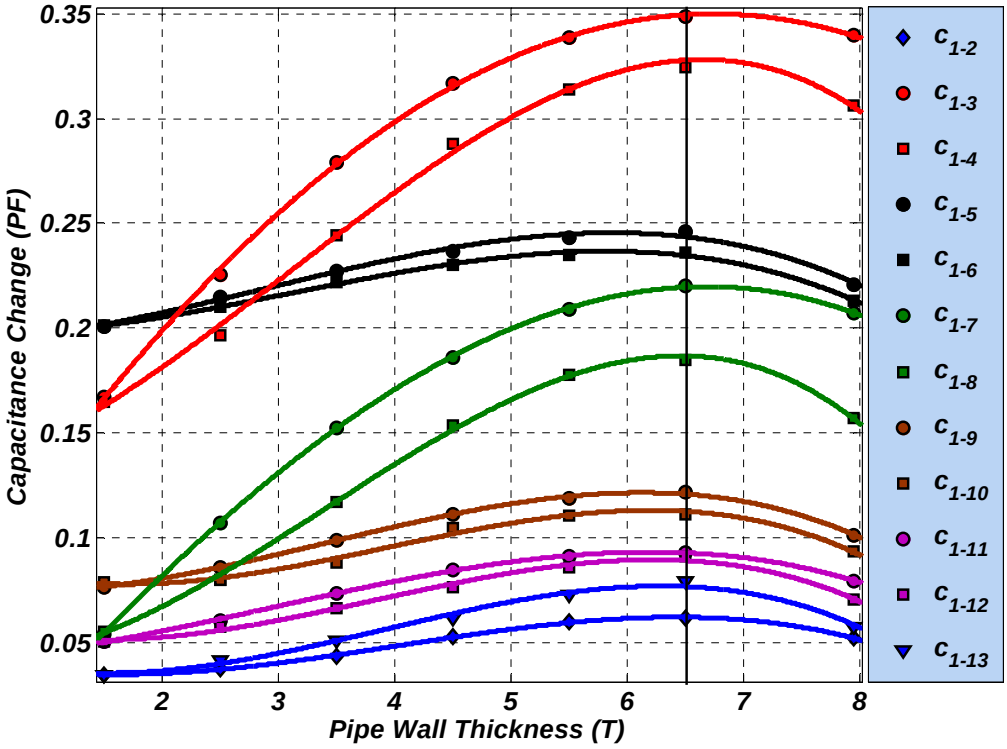

Fig.11 Expected Data of Capacitance change at θ = 40℃

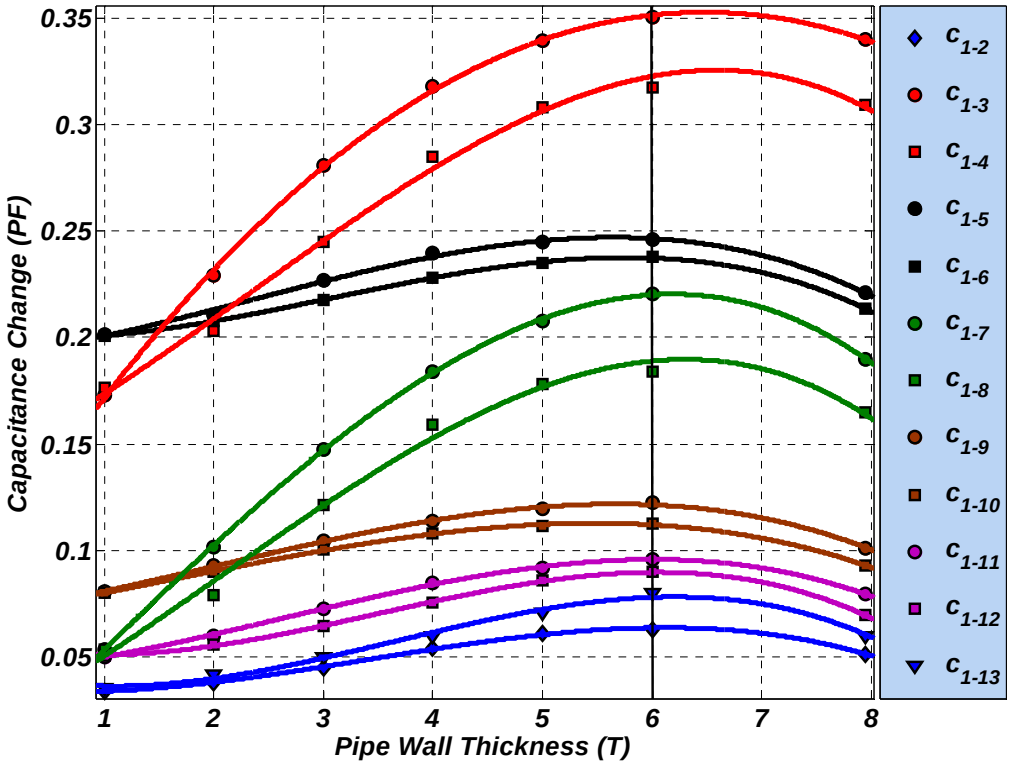

Fig.12 Expected Data of Capacitance change at $\theta = 60℃$

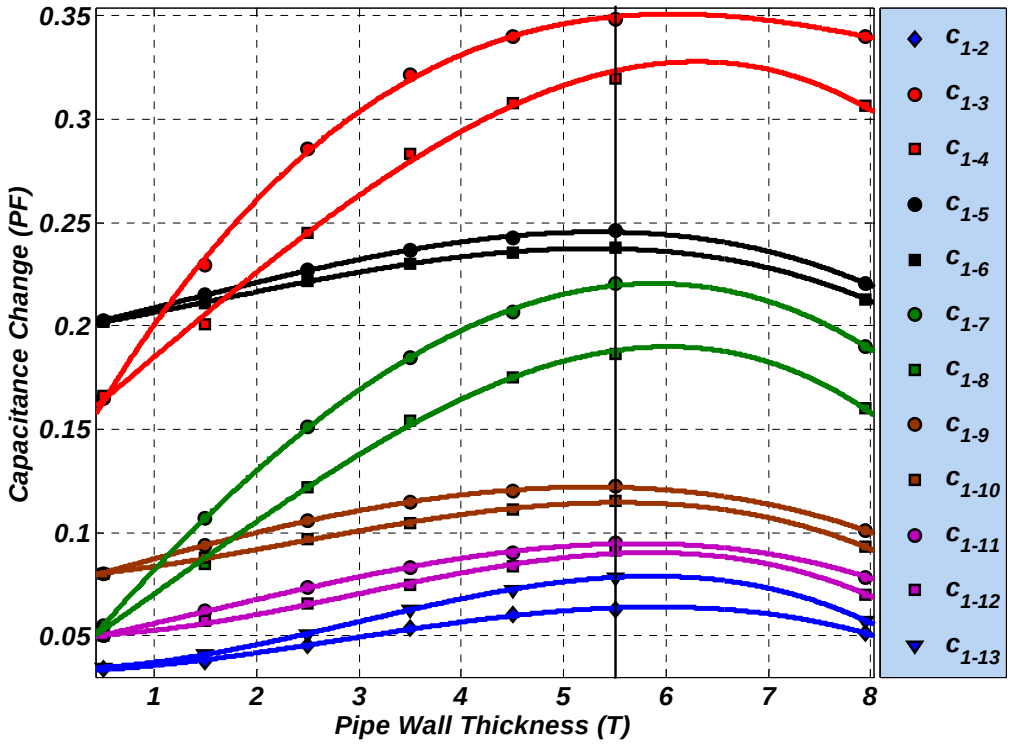

Fig.13 Expected Data of Capacitance change at $\theta = 80℃$

Table 3.Corrosion rate Constants (a_{ij}), (b_{ij}), (k_{ij}) and (h_{ij}) at $\theta = 25℃, 40℃, 60℃$ and $80℃$

	θ	C_{1-2}	C_{1-3}	C_{1-4}	C_{1-5}	C_{1-6}	C_{1-7}	C_{1-8}	C_{1-9}	C_{1-10}	C_{1-11}	C_{1-12}	C_{1-13}
a_{ij}	*25℃	**-7867**	**-1107**	**-1533**	**-2860**	**-3277**	**-4094**	**-4718**	**-5964**	**-6254**	**-6823**	**-7072**	**-7643**
	**40℃	-7713	-952	-1376	-2691	-3125	-3942	-4562	-5805	-6100	-6668	-6918	-7485
	**60℃	-7396	-632	-1054	-2372	-2806	-3623	-4241	-5493	-5785	-6353	-6593	-7173
	**80℃	-7172	-413	-832	-2158	-2581	-3411	-4028	-5272	-5552	-6126	-6372	-6951
$b_{ij} \times 10^{-4}$	*25℃	**-0.1907**	**-0.1987**	**-0.1967**	**-0.1938**	**-0.1921**	**-0.1953**	**-0.1928**	**-0.1973**	**-0.1980**	**-0.1972**	**-0.1924**	**-0.1983**
	**40℃	-0.1923	-0.1997	-0.1955	-0.1923	-0.1912	-0.1942	-0.1936	-0.1922	-0.1911	-0.1958	-0.1966	-0.1998
	**60℃	-0.1979	-0.1982	-0.1927	-0.1931	-0.1953	-0.1966	-0.1919	-0.1925	-0.1995	-0.1969	-0.1939	-0.1974
	**80℃	-0.1958	-0.1959	-0.1986	-0.1924	-0.1972	-0.1939	-0.1923	-0.1982	-0.1988	-0.1917	-0.1987	-0.1961
	Avg.	**-0.1942**	**-0.1981**	**-0.1959**	**-0.1929**	**-0.194**	**-0.195**	**-0.1926**	**-0.1951**	**-0.1969**	**-0.1954**	**-0.1954**	**-0.1979**
	S.D.	**0.0033**	**0.0016**	**0.0025**	**0.0007**	**0.0028**	**0.0012**	**0.0007**	**0.0031**	**0.0039**	**0.0025**	**0.0028**	**0.0016**
k_{ij}	*25℃	**7867**	**1107**	**1533**	**2860**	**3277**	**4094**	**4718**	**5964**	**6254**	**6823**	**7072**	**7643**
	**40℃	7713	952	1376	2691	3125	3942	4562	5805	6100	6668	6918	7485
	**60℃	7396	632	1054	2372	2806	3623	4241	5493	5785	6353	6593	7173
	**80℃	7172	413	832	2158	2581	3411	4028	5272	5552	6126	6372	6951
$h_{ij} \times 10^{-4}$	*25℃	**0.1921**	**0.1986**	**0.1977**	**0.1927**	**0.1960**	**0.1964**	**0.1976**	**0.1978**	**0.1903**	**0.1929**	**0.1995**	**0.1973**
	**40℃	0.1956	0.1945	0.1945	0.1941	0.1921	0.1949	0.1932	0.1998	0.1982	0.1941	0.1925	0.1946
	**60℃	0.1962	0.1969	0.1987	0.1911	0.1982	0.1962	0.1925	0.1999	0.1913	0.1964	0.1987	0.1997
	**80℃	0.1933	0.1948	0.1964	0.1987	0.1949	0.1942	0.1928	0.1983	0.1920	0.1981	0.1922	0.1921
	Avg.	**0.1943**	**0.1962**	**0.1968**	**0.1942**	**0.1953**	**0.1954**	**0.194**	**0.199**	**0.193**	**0.1954**	**0.1957**	**0.1959**
	S.D.	**0.0019**	**0.0019**	**0.0018**	**0.0033**	**0.0025**	**0.0011**	**0.0024**	**0.0011**	**0.0036**	**0.0023**	**0.0039**	**0.0033**
C.F	*25℃	**0.9945**	**0.9921**	**0.9908**	**0.9369**	**0.9928**	**0.9701**	**0.9828**	**0.9628**	**0.9043**	**0.9946**	**0.9715**	**0.9932**
	**40℃	0.9994	0.9995	0.9976	0.9921	0.9948	0.9999	0.9989	0.9983	0.9855	0.9993	0.9911	0.9897
	**60℃	0.998	0.9994	0.9946	0.9939	0.9991	0.9999	0.9921	0.9987	0.9963	0.9994	0.9993	0.9903
	**80℃	0.9977	0.9992	0.9973	0.999	0.9993	0.9999	0.9988	0.9991	0.9984	0.9993	0.9955	0.9999

*** FEM Data**

**** FFNN Expected Data**

6. CONCLUSION

For this work, the finite element method (FEM) and artificial neural network (ANN) techniques were used for modeling and simulating the electrical capacitance tomography (ECT) sensor to detect the corrosion rates inside steel pipelines and study and predict the effect of pipeline environment temperature (θ) on the corrosion rates, the following conclusions can be drawn:

1) The pipeline internal corrosion is means decrease of the pipeline thickness was discussed completely by FEM numerical simulation software ANSYS. The influence of pipeline to electrode pairs decreases followed by ($C_{1\text{-}3}$, $C_{1\text{-}4}$, $C_{1\text{-}5}$, $C_{1\text{-}6}$, $C_{1\text{-}7}$, $C_{1\text{-}8}$, $C_{1\text{-}9}$, $C_{1\text{-}10}$, $C_{1\text{-}11}$, $C_{1\text{-}12}$, $C_{1\text{-}13}$ and $C_{1\text{-}2}$). Maximum capacitance change is gotten at X = 6.95 mm, ρ = 0.79, which is beneficial for capacitance measurement. With the decrease of pipe wall thickness (X) or decrease of the radius-electrode ratio (ρ), the distortion of ECT sensor sensitivity becomes more serious.
2) An artificial neural network can be used as a method for simulating the ECT sensor to expect the non-FE Data of capacitance change at the pipeline environment temperature $\theta = 25℃, 40℃, 60℃$ and $80℃$.
3) Training a neural network is heavily time consuming.
4) Using the exponential formula $C_{ij} = a_{ij}e^{b_{ij}X} + k_{ij}e^{h_{ij}X}$ has proved its suitability for present study, and it is found that, the deviation of the constants (b_{ij} & h_{ij}) for different pipeline environment temperature (θ) and capacitance change (C_{ij}) is negligible and it may be considered to be constant.
5) The value of the constants (a_{ij} & k_{ij}) were found to be depend on the pipeline environment temperature (θ) and the capacitance change (C_{ij}) with high correlation factors (C.F), as the pipeline environment temperature (θ) increases the value of (a_{ij} & k_{ij}) will decreases i.e. the pipeline environment temperature (θ) had a detrimental effect on the corrosion rates increases.

REFERENCES

Fasching, G.E.; Smith, N.S., (1988), “High Resolution Capacitance Imaging System”, US Dept. Energy, 37, DOE/METC-88/4083

Fasching, G.E.; Smith, N.S., (1991) “A Capacitive System for 3-Dimensional Imaging of Fluidized-Beds”, Rev. Sci. Instr., 62, 2243-2251

Yang W. Q., et al., (1995a), “Development of capacitance tomographic imaging systems for oil pipeline measurements”, Review of Scientific Instruments, 66(8), pp. 4326

Yang W. Q., et al., (1995b), “Electrical capacitance tomography –from design to applications”, Measurement & Control, 28(9), pp. 261-266

Li Haiqing et al., (2000), “Special measurement technology and application”, Hangzhou: Zhejiang University Press

Yang W. Q., et al., (1999), “New AC-based capacitance tomography system”, IEE proceedings: Measurement Science and Technology, 146(1), pp.47-53.

Yang W. Q., et al., (1997), “Modelling of capacitance sensor”, IEE proceedings: Measurement Science and Technology, 144(5), pp. 203-208.

Jaworski A. J., et al., (2000), “The design of an electrical capacitance tomography sensor for use with media of high dielectric permittivity”, Measurement Science and Technology, 11(6), pp. 743-757

Xie, et al., (1992), “Electrical capacitance tomography for flow imaging: system model for development of image reconstruction algorithms and design of primary sensors”, IEE Proceedings-G, 139(1): 89-98